A Comprehensive Analysis of the NADP-Malic Enzyme Gene Family of Arabidopsis[1][w]

Mariel C. Gerrard Wheeler, Marcos A. Tronconi, María F. Drincovich, Carlos S. Andreo*, Ulf-Ingo Flügge, and Verónica G. Maurino

Centro de Estudios Fotosintéticos y Bioquímicos (CEFOBI), Universidad Nacional de Rosario, Rosario, Argentina (M.C.G.W., M.A.T., M.F.D., C.S.A.); and Botanisches Institut, Universität zu Köln, D–50931 Cologne, Germany (U.-I.F., V.G.M.)

The Arabidopsis (*Arabidopsis thaliana*) genome contains four genes encoding putative NADP-malic enzymes (MEs; *AtNADP-ME1–ME4*). NADP-ME4 is localized to plastids, whereas the other three isoforms do not possess any predicted organellar targeting sequence and are therefore expected to be cytosolic. The plant NADP-MEs can be classified into four groups: groups I and II comprising cytosolic and plastidic isoforms from dicots, respectively; group III containing isoforms from monocots; and group IV composed of both monocots and dicots, including AtNADP-ME1. AtNADP-MEs contained all conserved motifs common to plant NADP-MEs and the recombinant isozymes showed different kinetic and structural properties. NADP-ME2 exhibits the highest specific activity, while NADP-ME3 and NADP-ME4 present the highest catalytic efficiency for NADP and malate, respectively. NADP-ME4 exists in equilibrium of active dimers and tetramers, while the cytosolic counterparts are present as hexamers or octamers. Characterization of T-DNA insertion mutant and promoter activity studies indicates that NADP-ME2 is responsible for the major part of NADP-ME activity in mature tissues of Arabidopsis. Whereas NADP-ME2 and -ME4 are constitutively expressed, the expression of NADP-ME1 and NADP-ME3 is restricted by both developmental and cell-specific signals. These isoforms may play specific roles at particular developmental stages of the plant rather than being involved in primary metabolism.

Malic enzymes (MEs) catalyze the oxidative decarboxylation of L-malate, producing pyruvate, CO_2, and NAD(P)H in the presence of a divalent cation (Chang and Tong, 2003). This enzyme is widely distributed in nature due to the participation of the reaction products in a large number of metabolic pathways (Lance and Rustin, 1984). In plants, NAD-dependent isoforms (NAD-ME; EC 1.1.1.39) function predominantly in mitochondria to produce pyruvate for oxidation in the tricarboxylic acid cycle (Artus and Edwards, 1985), while NADP-dependent MEs (NADP-ME; EC 1.1.1.40) are found in cytosol and plastids (Edwards and Andreo, 1992; Drincovich et al., 2001). Thus, different NADP-ME isoforms have been found in bundle sheath chloroplasts of some C_4 plants and in the cytosol of some Crassulacean acid metabolism (CAM) plants, where they take part in the photosynthetic metabolism, as well as in the cytosol and plastids of photosynthetic and nonphotosynthetic tissues of C_3, C_4, and CAM plants playing different postulated non-photosynthetic roles (Drincovich et al., 2001; Lai et al., 2002a, 2002b).

The biological role of NADP-MEs, apart from being involved in C_4 and CAM photosynthesis, remains elusive. Plastidic nonphotosynthetic isoforms were suggested to be involved in plant defense responses (Casati et al., 1999) and in lipid biosynthesis by providing carbon skeletons and reducing power (Smith et al., 1992; Eastmond et al., 1997). Cytosolic isoforms have also been linked to plant defense responses (Schaaf et al., 1995) and, in addition, to lignin biosynthesis by providing NADPH (Schaaf et al., 1995) and to control the cytosolic pH by balancing the synthesis and degradation of malate (Martinoia and Rentsch, 1994). Another suggested role for the NADP-ME is the control of stomatal closure by degrading malate during the day (Outlaw et al., 1981; Laporte et al., 2002). Results from in situ immunolocalization studies indicate the occurrence of a cytosolic NADP-ME isoform in guard cell complexes of the C_3 plant wheat (Maurino et al., 1997). Nevertheless, the complete set of NADP-ME isoforms in plants has not yet been thoroughly analyzed. Such studies will shed light on the biological function of both plastidic and cytosolic isoforms in the same tissue or different NADP-MEs sharing the same subcellular compartment. A recent work reveals the occurrence of four NADP-ME isoforms in the monocot rice (*Oryza sativa*; Chi et al., 2004), although none of the isoforms was characterized either at the biochemical or at the expression levels. Several cytosolic and plastidic photosynthetic and nonphotosynthetic NADP-ME transcripts were

[1] This work was supported by the Agencia Nacional de Promoción Científica y Tecnológica (PICT 1–11604, Argentina), Fundación Antorchas (project no. 4248–63, Argentina), SeCyt-DAAD (DA/PA05–BI/016), and CONICET (PIP 3029) as well as the Deutsche Forschungsgemeinschaft (to V.G.M.).

* Corresponding author; e-mail candreo@fbioyf.unr.edu.ar; fax 54–341–4370044.

[w] The online version of this article contains Web-only data.

Article, publication date, and citation information can be found at www.plantphysiol.org/cgi/doi/10.1104/pp.105.065953.

detected in *Flaveria* sp. that display different C_3 and C_4 photosynthetic pathways (Lai et al., 2002a, 2002b).

The complete Arabidopsis (*Arabidopsis thaliana*) genome presents the opportunity to study the whole set of NAD(P)-ME isoforms present in this C_3 dicot plant (Arabidopsis Genome Initiative, 2000). Sequence data and homology searches show that the Arabidopsis genome contains two *NAD-ME* genes and four *NADP-ME* genes. To characterize the *AtNADP-ME* gene family, cDNAs encoding the four NADP-ME isoforms were cloned, expressed in a prokaryotic system, and the proteins obtained were structurally and biochemically characterized. In addition, insertion mutants defective in particular NADP-ME activity were characterized and tissue-specific expression patterns for the individual genes were obtained by promoter-β-glucuronidase (GUS) fusions. Based on these results, possible novel roles for some members of the NADP-ME family in Arabidopsis are discussed.

RESULTS

Cloning and In Silico Analysis of the AtNADP-ME Family

Four putative *AtNADP-ME* genes were identified as orthologs to the nonphotosynthetic maize *NADP-ME* (AY315822; Maurino et al., 2001) and named *NADP-ME1* (At2g19900), *NADP-ME2* (At5g11670), *NADP-ME3* (At5g25880), and *NADP-ME4* (At1g79750). Computational sorting prediction programs (ChloroP V1.1 and TargetP Server v1.01; Emanuelsson et al., 1999) indicate that NADP-ME4 contains a putative plastidic transit peptide (pTP) of about 74 amino acid residues in length, directing the protein to the plastids. Comparison of the *NADP-ME4* genomic and cDNA sequences revealed that the region encoding the putative transit peptide contains an intron at position 31. NADP-ME1 to -ME3 do not contain any predicted organelle sorting signal.

Within the AtNADP-ME family, the predicted amino acid sequences showed identities between 78% (NADP-ME1 versus NADP-ME4) and 91% (NADP-ME2 versus NADP-ME3). A multiple alignment with known NADP-MEs showed that all NADP-MEs, including the AtNADP-MEs, contained conserved motifs (data not shown; Drincovich et al., 2001). The four putative AtNADP-ME isoforms were included in a phylogenetic tree constructed with the whole set of complete plant NADP-ME sequences (Fig. 1). In addition to the sequences previously analyzed (Drincovich et al., 2001) and the four AtNADP-MEs, six new NADP-ME sequences are included. The plant NADP-MEs can obviously be classified into four groups: the AtNADP-ME2 and NADP-ME3 group into the cytosolic dicot NADP-ME group (group I), while AtNADP-ME4 is included in the plastidic dicot NADP-ME group (group II). Neither of the AtNADP-ME isoforms group into the monocot NADP-MEs (group III). The novel group IV comprises both monocot and dicot enzymes, including AtNADP-ME1.

NADP-ME4 Is Localized to Plastids

To obtain experimental evidence for the functionality of the predicted pTP of NADP-ME4, the region encoding the putative pTP was fused in frame to the green fluorescent protein (GFP) coding sequence. As shown in Figure 2A, the first 252 nucleotides of NADP-ME4 were able to direct GFP to the plastids in transient transfection assays using tobacco (*Nicotiana tabacum*) BY-2 protoplasts (Fig. 2A). A control using the GFP coding region shows localization of the free GFP to cytosolic and nuclear compartments (Fig. 2A).

Heterologous Expression and Biochemical Characterization of Recombinant AtNADP-ME Isoforms

To assess whether the four predicted *AtNADP-ME* cDNAs encode enzymatically active NADP-ME proteins, the different NADP-ME isoforms were expressed in *Escherichia coli* (in the case of NADP-ME4, without the pTP) and purified to homogeneity. Following induction by isopropylthio-β-galactoside or lactose, the *E. coli* BL21 strain transformed with pET-ME1, pET-ME2, pET-ME3, or pET-ME4 showed the presence of expressed proteins with the expected molecular masses of approximately 80 kD (approximately 65 kD of the NADP-ME isoforms plus an approximately 17-kD fragment coded for by the expression vector; Fig. 3A, lane 1). Fusion proteins were subsequently purified by His-bind affinity chromatography. After enterokinase digestion of each protein to remove the His-tag, products of approximately 65 kD were obtained representing the mature proteins (Fig. 3A, lanes 2–4). In western-blot assays, the four recombinant AtNADP-MEs reacted with antibodies against recombinant maize (*Zea mays*) NADP-ME (data not shown).

Figure 3B presents results obtained by native electrophoresis of the purified recombinant AtNADP-MEs. As a control, the tetrameric maize recombinant photosynthetic NADP-ME was analyzed (Detarsio et al., 2003). Activity staining assays indicate that NADP-ME4, the plastidic isoform, exists in equilibrium of active tetramers and dimers, as the molecular masses of the active bands are consistent with these oligomeric states (approximately 260 and 130 kD). Interestingly, the native molecular masses of the cytosolic isoforms (NADP-ME1, NADP-ME2, and NADP-ME3) are higher than the 400 kD indicative for higher oligomeric states of these isoenzymes, probably hexamers or octamers.

Recombinant purified NADP-ME1, NADP-ME2, NADP-ME3, and NADP-ME4 were characterized with respect to kinetic properties (Table I). The isoforms that presented the highest specific activities were the cytosolic forms NADP-ME2 followed by NADP-ME3. The specific activity of NADP-ME2 was more than twice as high as that obtained for NADP-ME4 and more than 8 times the value for NADP-ME1. Comparing the K_m (NADP) values, NADP-ME3 and NADP-ME4 exhibit the highest affinity toward NADP (6–10 μM),

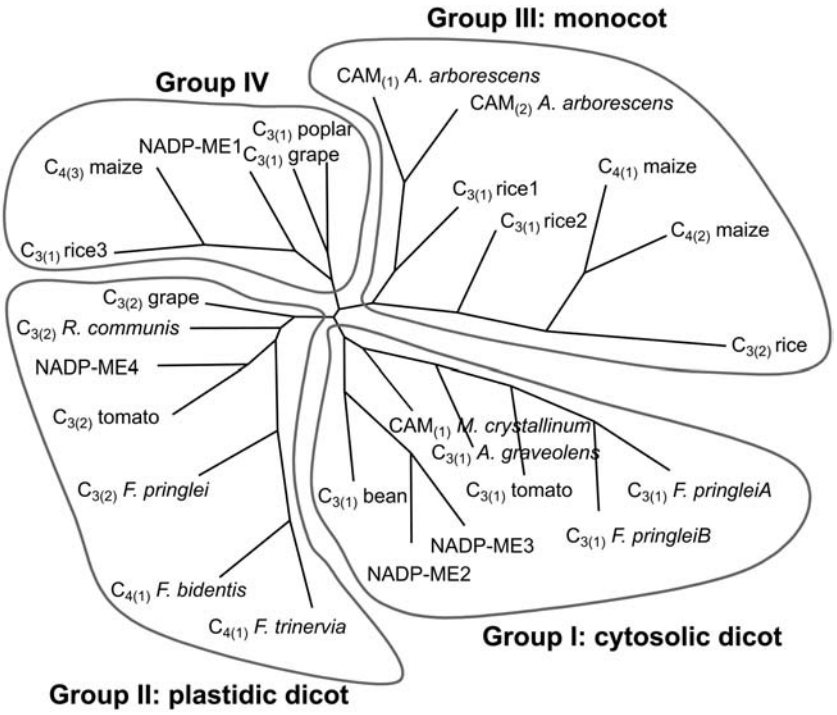

Figure 1. Phylogenetic tree of plant NADP-ME. Mature proteins were aligned using ClustalW (1.81) and the alignment obtained was modified by visual inspection to exclude the sites containing gaps. The phylogenetic tree was constructed by the neighbor-joining (NJ) method. Statistical significance of each branch of the tree was evaluated by bootstrap analysis by 100 iterations of bootstrap samplings and reconstruction of trees by the NJ method. The topology obtained by this method is shown. The following sequences, in addition to the four Arabidopsis NADP-MEs, were analyzed: $C_{4(1)}$-NADP-ME from maize (Rothermel and Nelson, 1989), *Flaveria trinervia* (Borsch and Westhoff, 1990), and *Flaveria bidentis* (AY863144); $C_{4(2)}$-NADP-ME from maize (Saigo et al., 2004); $C_{4(3)}$-NADP-ME from maize (AY864063); CAM_1-NADP-ME from *Mesembryanthemum crystallinum* (Cushman, 1992) and *Aloe arborescens* (Honda et al. 2000); CAM_2-NADP-ME from *A. arborescens* (Honda et al., 1997); $C_{3(1)}$-NADP-ME from bean (*Phaseolus vulgaris*; Walter et al., 1990), poplar (*Populus* spp.; van Doorsseleare et al., 1991), grape berries (Franke and Adams, 1995), tomato (*Lycopersicon esculentum*; AF001270), *Apium graveolens* (AJ132257), *F. pringlei* (Lai et al., 2002a), and rice ($C_{3(1)}$ rice1, rice2, and rice3; Chi et al., 2004); $C_{3(2)}$-NADP-ME from rice (Fushimi et al., 1994), *F. pringlei* (Lipka et al., 1994), tomato (AF001269), grape berries (U67426), and *Ricinus communis* (AF262997). The photosynthetic isoforms were named as $C_{4(1)}$-NADP-ME and CAM_1-NADP-ME; the plastidic nonphotosynthetic NADP-ME isoforms as $C_{4(2)}$-NADP-ME and $C_{3(2)}$-NADP-ME, while the nonphotosynthetic cytosolic isoforms as $C_{4(3)}$-NADP-ME, CAM_2-NADP-ME, and $C_{3(1)}$-NADP-ME (Drincovich et al., 2001).

followed by NADP-ME2 (approximately 70 μM), and NADP-ME1 with the lowest affinity of all NADP-MEs characterized up to now (approximately 200 μM; Drincovich et al., 2001). In summary, NADP-ME3 presents the highest catalytic efficiency (k_{cat}/K_m) with NADP, which is more than twice as high as that of NADP-ME4, almost 1 order of magnitude higher than that of NADP-ME2 and more than 2 orders of magnitude higher as compared to NADP-ME1. On the other hand, when comparing the K_m (malate) values, the plastidic isoform (NADP-ME4) presents the highest affinity. In this regard, the kinetic behavior obtained with respect to malate was nonhyperbolic only for NADP-ME1, presenting some kind of sigmoidicity (Table I).

Expression Analysis of the Arabidopsis NADP-ME Genes

Semiquantitative reverse transcription (RT)-PCR was conducted to analyze the expression of *NADP-ME* in different tissues of Arabidopsis. *NADP-ME2* and *NADP-ME4* transcripts are present in all organs tested, whereas *NADP-ME1* is preferentially expressed in roots (Fig. 2B). By contrast, *NADP-ME3* transcripts are hardly detectable in roots, while mRNA abundance is higher in flowers (Fig. 2B). To further investigate the expression of *AtNADP-MEs*, publicly available microarray data were also analyzed (http://www.genevestigator.ethz.ch; Zimmermann et al., 2004). These data support the RT-PCR analyses (Fig. 2B) and the promoter::GUS expression data shown below.

To allow a more thorough analysis of *AtNADP-ME* gene expression during plant development, translational fusions of the promoter sequences, the first exon and intron, and part of the second exon with the *uidA* (*GUS*) gene were stably introduced into Arabidopsis. All the T1 plants selected showed the same qualitative expression pattern. T2 plants from at least six independent transformants per construct were analyzed histochemically for GUS activity.

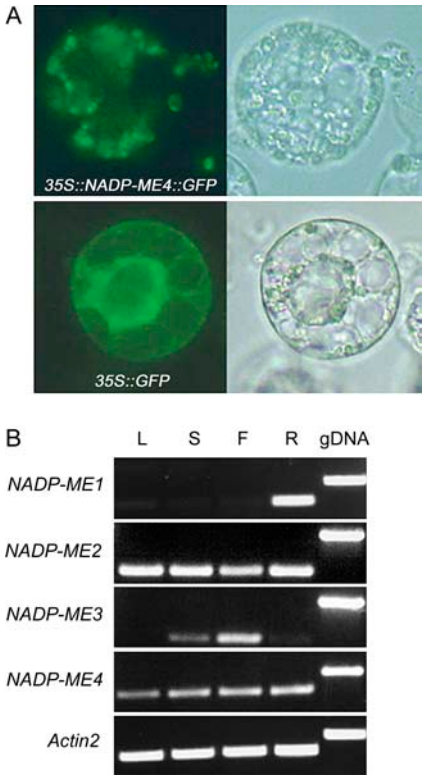

Figure 2. Expression analysis of NADP-ME. A, Transient expression of NADP-ME4::GFP in transfected protoplasts. Tobacco BY-2 protoplasts were transfected with a plasmid bearing the genes *35S::NADP-ME4::GFP* (top) or *35S::GFP* (bottom). Fluorescence distribution (left) indicates localization of the NADP-ME4::GFP to plastids and of free GFP to the cytosolic and nuclear compartments. Bright-field images are shown at the right. Diameter of protoplasts is approximately 30 μm. B, Semiquantitative RT-PCR. RNA from different tissues (L, leaf, S, stem; F, flower; R, root) of Arabidopsis was transcribed to cDNA. A 271-bp fragment of NADP-ME1, a 177-bp fragment of NADP-ME3, and a 268-bp fragment of NADP-ME4 were amplified by 35 cycles. A 223-bp fragment of NADP-ME2 was amplified by 29 cycles. As loading control, a 607-bp Actin2 fragment was amplified by 29 cycles. As control for purity, genomic DNA (gDNA) resulted in amplification products of 454, 431, 380, 356, and 685 bp, respectively.

Expression during Embryogenesis

NADP-ME1::GUS-expressing lines showed very strong GUS staining only in the embryo from the torpedo stage onward (Fig. 4, a–d). Pods did not show staining (data not shown). In the NADP-ME2::GUS and NADP-ME3::GUS lines, low GUS staining could be detected in the embryo at the globular and heart stages (Fig. 4, e–l). In the case of NADP-ME2, expression was also observed in the funiculus (Fig. 4e) and vascular tissues of the siliques (data not shown), whereas in NADP-ME3::GUS activity was found in the central vasculature of the siliques (data not shown). Strong GUS staining was detected in the NADP-ME4::GUS-expressing lines in the endosperm and the embryo at all developmental stages, including the seed attachment point and the integuments (Fig. 4, m–p). Pods also showed GUS activity throughout the tissue (data not shown).

Expression during Germination

The expression pattern of the four *AtNADP-ME* genes was analyzed during the first 2 weeks after imbibition. It is worth mentioning that, due to the high level of expression, incubation of the seedlings between 2 and 6 d after imbibition (DAI) with GUS staining solution was performed between 30 min and 1 h at 37°C. Two DAI, NADP-ME1::GUS expression was restricted to the radicle (Fig. 5a) and became more pronounced in the root tip by 4 DAI (Fig. 5b). Hypocotyl and cotyledons showed GUS expression by 5 DAI onward, while the expression tends to disappear from the root tissue. No GUS staining was evident in the primary leaves (Fig. 5c). At 2 DAI, GUS expression directed by the *NADP-ME2* promoter was restricted to the proximal part of the radicle having root hairs (Fig. 5d). During the next days, strong staining expanded toward the meristematic region, except for the root tip (Fig. 5e). Strong expression was obtained in hypocotyls

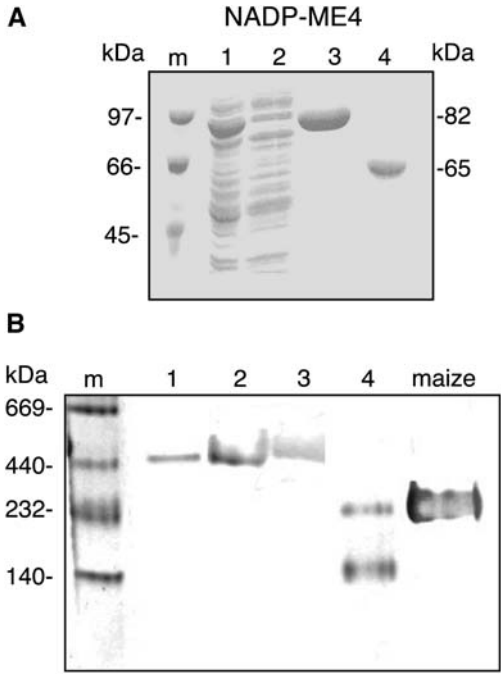

Figure 3. Recombinant Arabidopsis NADP-ME isoforms analyzed by gel electrophoresis. A, Coomassie-stained SDS-PAGE of recombinant NADP-ME isoforms. Lane 1, 20 μg of *E. coli* crude extract expressing NADP-ME4 after lactose or IPTG induction; lane 2, wash of the Ni-NTA column; lanes 3 and 4, 5 μg of purified recombinant NADP-ME4 before (3) and after (4) enterokinase digestion. After the Ni-NTA column, the proteins were digested and further purified by affinity chromatography (Affi Gel Blue). The estimated molecular mass of the purified proteins is indicated on the right. Similar protein patterns were obtained for NADP-ME1, NADP-ME2, and NADP-ME3. m, M_r markers. B, Native PAGE of recombinant NADP-ME isoforms. Approximately 5 milliunits of each recombinant purified isoform were loaded. Lane 1, NADP-ME1; lane 2, NADP-ME2; lane 3, NADP-ME3; lane 4, NADP-ME4. Maize, Recombinant maize photosynthetic NADP-ME. The native gel was stained for NADP-ME activity as described in "Materials and Methods." M_r markers were run in parallel (m).

Table I. *Kinetic properties of recombinant Arabidopsis NADP-ME isoforms*

The indicated values, obtained by nonlinear regression, are the average of at least three different measurements ± SE with the same batch of recombinant enzymes. At least one additional batch of enzymes was used in each case with high reproducibility, obtaining values with less than 8% difference from the values indicated in the table.

	NADP-ME1	NADP-ME2	NADP-ME3	NADP-ME4
$k_{cat,NADP}$ (s^{-1})	38.7 ± 3.5	324.1 ± 29.2	268.1 ± 24.1	151.3 ± 12.1
K_m NADP (μM)	205.1 ± 22.6	72.1 ± 7.2	6.5 ± 0.62	10.2 ± 1.2
k_{cat}/K_m NADP	0.19	4.5	41.2	14.8
K_m malate (mM)	2.96[a] ± 0.33	3.33 ± 0.37	0.83 ± 0.09	0.23 ± 0.025
k_{cat}/K_m malate	13.0	97.3	323.0	657.8

[a] $S_{0.5}$ (n_H = 2.0).

and cotyledons 6 DAI when the seedlings were incubated for more than 1 h in the staining solution. Primary leaves also showed GUS expression (Fig. 5f). GUS activity could not be detected in NADP-ME3::GUS lines at any stages of germination (Fig. 5, g and h). At later stages, GUS staining could be observed in stipules at the shoot apex and restricted to trichomes of the primary leaves (Fig. 5i). In the case of NADP-ME4::GUS lines, GUS expression was confined to the radicle 2 DAI (Fig. 5j) also approaching the meristematic region 3 DAI. At 4 DAI, the whole root was strongly stained and a low expression was also visible in the cotyledons when incubated in the staining solution for not longer than 1 h (Fig. 5k). By increasing the incubation time, strong expression was also seen in cotyledons. In contrast to the hypocotyls, the cotyledons displayed a strong GUS expression 7 DAI and this pattern was maintained with the appearance of true leaves (Fig. 5l).

Expression in Vegetative Organs

NADP-ME1::GUS plants showed GUS expression only in some secondary roots, where it was confined to the stele (Fig. 6a) and excluded from the tips (data not shown). No GUS activity was detectable in leaves and stems throughout growth (data not shown). In NADP-ME2::GUS plants, reporter gene activity was found in all vegetative organs. Roots showed expression throughout all the tissues, except for root tips (Fig. 6b).

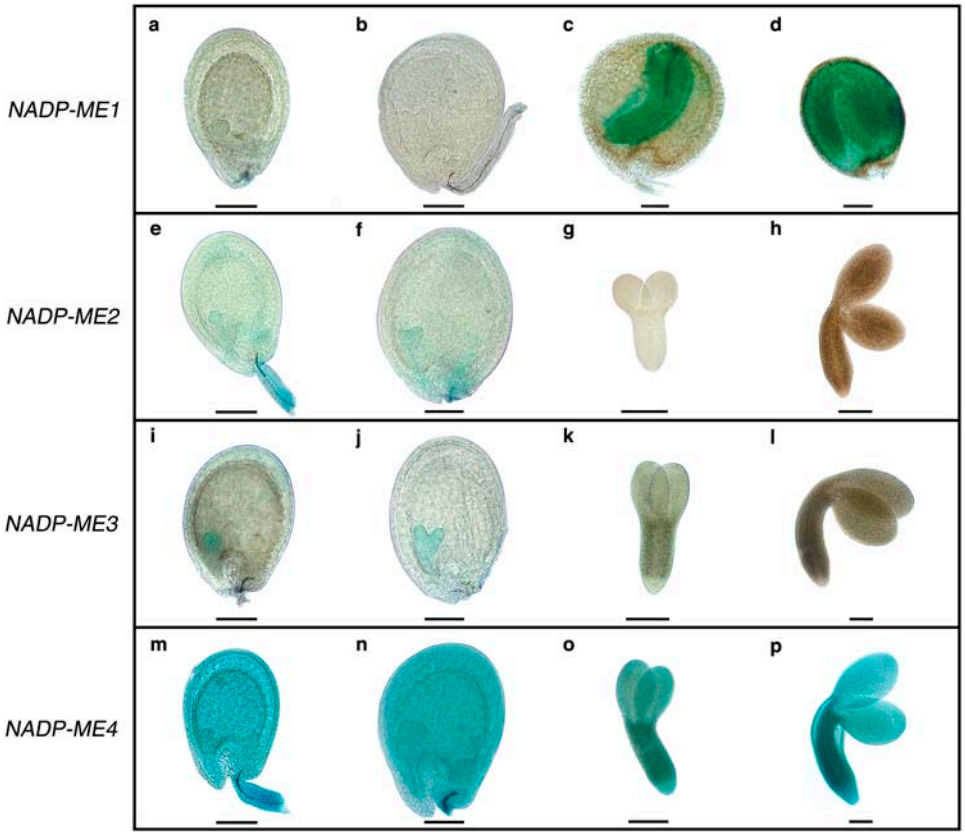

Figure 4. Analysis of *AtNADP-ME*::*GUS* expression during embryogenesis. a to d, *NADP-ME1*::*GUS* expression in seeds at the globular, heart, linear cotyledon, and mature embryo stages. e to h, *NADP-ME2*::*GUS* expression in seeds at the globular, heart, torpedo, and mature embryo stages. i to j, *NADP-ME3*::*GUS* expression in seeds at the globular, heart, linear cotyledon, and mature embryo stages. m to p, *NADP-ME4*::*GUS* expression in seeds at the globular, heart, linear cotyledon, and mature embryo stages. Scale bars represent 100 μm.

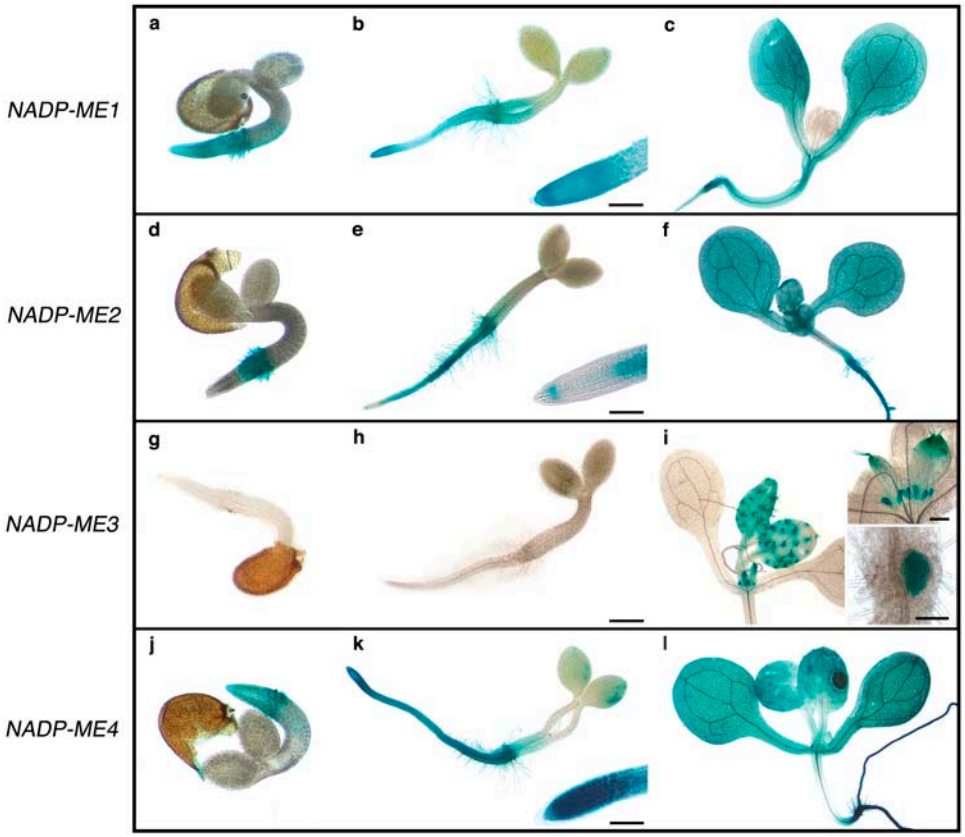

Figure 5. Analysis of *AtNADP-ME*::*GUS* expression during germination. a to c, *NADP-ME1*::*GUS* expression after 2, 4, and 10 DAI. d to f, *NADP-ME2*::*GUS* expression after 2, 4, and 10 DAI. g to i, *NADP-ME3*::*GUS* expression after 2, 4, and 12 DAI. j to l, *NADP-ME4*::*GUS* expression after 2, 4, and 14 DAI. Scale bars represent 50 μm.

Leaves exhibited GUS activity in all cell types, being particularly strong in the trichome basal cells and hydatodes (Fig. 6e). Stems showed strong GUS staining particularly in the vasculature (Fig. 6h). GUS expression was restricted to the trichomes and trichome basal cells of leaves and stems of NADP-ME3::GUS plants (Fig. 6, f and i). Interestingly, these plants showed expression of the NADP-ME3::GUS fusion in the stipules flanking the base of the inflorescence bract leaves (Fig. 6f) and the meristematic zone of developing lateral roots (Fig. 6c). NADP-ME4::GUS expression was found in all vegetative organs. Roots of these transgenic plants showed GUS staining in the stele, including the vascular tissue and the pericycle, mainly at emerging lateral roots and at root tips (Fig. 6d). In leaves and stems, GUS expression was also more intense in the vascular system (Fig. 6, g and j). NADP-ME4::GUS staining was found in guard cells of cotyledonous leaves, hypocotyls, and petioles (Fig. 6g). However, GUS activity was not obvious in guard cells of rosette and cauline leaves.

Expression in Reproductive Organs

GUS activity staining of inflorescences indicated that NADP-ME1::GUS is not expressed in the floral organs (data not shown). NADP-ME2::GUS was expressed in sepals and filaments of developed flowers (Fig. 6k). In developing siliques, GUS staining was found at both ends, the stigmatic papillae and the abscission zone. The expression of NADP-ME3::GUS was found exclusively in pollen from the latest maturation stages up to its germination on the stigma (Fig. 6l). It is worth mentioning that, due to the high expression level of NADP-ME3, the inflorescences were incubated for only 3 h in the staining solution. The abscission zone of developing siliques also displayed GUS activity. NADP-ME4::GUS plants presented GUS staining in sepals, stigma, filaments, or pollen of opened flowers (Fig. 6m).

Identification of *nadp-me* Insertional Lines

Several T-DNA mutants defective in the different *AtNADP-ME* genes could be identified in the SALK and SAIL collections. In all cases, homozygous lines were generated and confirmed using a PCR-based approach (data not shown). The position of the T-DNA insertion was determined by PCR amplification and sequencing of both ends of the insertion and of the flanking genomic DNA (Fig. 7A). Insertion line *nadp-me1* presented a concatemer insertion in the orientation left border (LB)-LB in intron 15 (positions 2419–2432). In the case of *nadp-me2*, the insertion was localized to exon 5 (positions 983–1012), with an orientation right border (RB)-LB. Two additional lines of *nadp-me2* were also analyzed. In the case of *nadp-me2a* and *2b*, insertions with the orientation LB-RB in intron

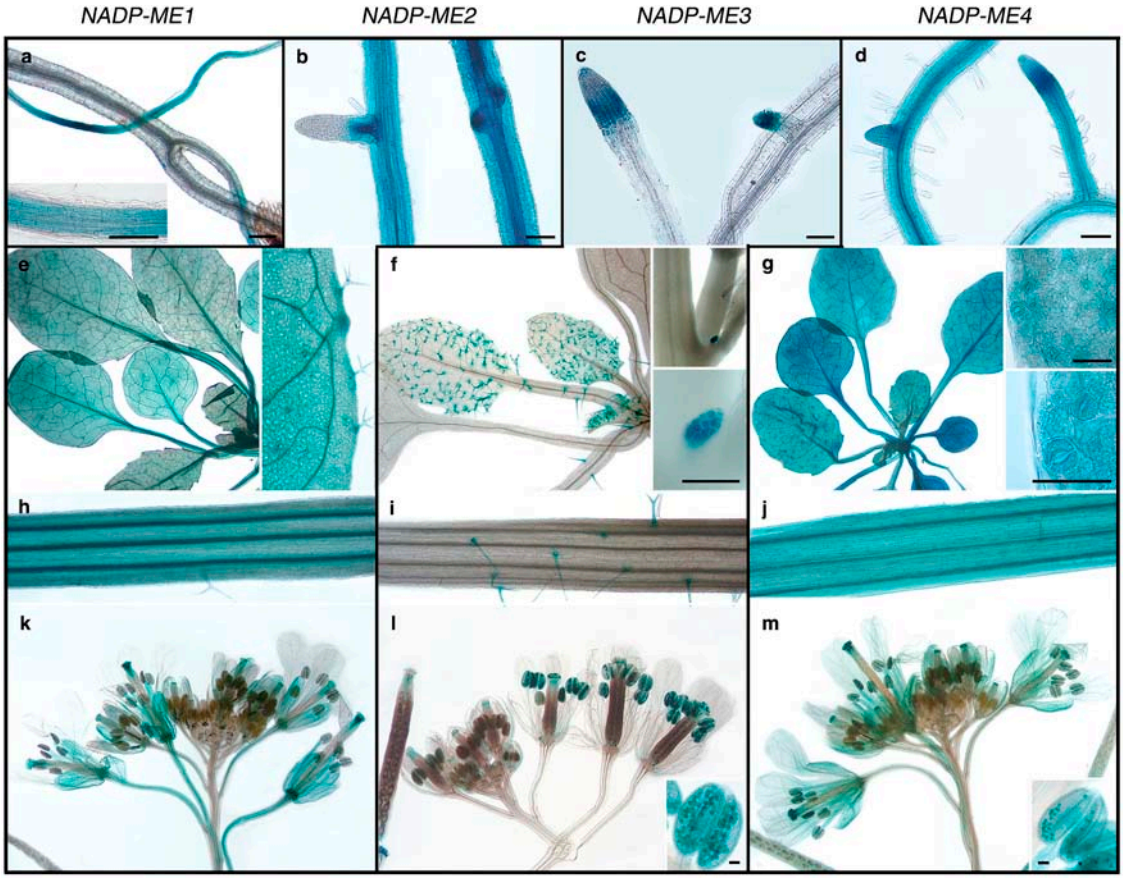

Figure 6. Analysis of *AtNADP-ME*::*GUS* expression in vegetative and reproductive organs. a to d, GUS expression in roots driven by *NADP-ME1*, *NADP-ME2*, *NADP-ME3*, and *NADP-ME4*, respectively. e, *NADP-ME2*-driven expression in the rosette of a 3-week-old seedling. Closeup of a leaf surface showing expression in trichome basal cells and hydathodes (inset). f, GUS expression in the trichomes of 3-week-old rosette leaves driven by *NADP-ME3*. GUS expression in the stipules of an inflorescence bract leaf (insets). g, *NADP-ME4* expression in leaves of a 3-week-old seedling. Staining in the guard cells of cotyledons is shown in the insets. h to j, Longitudinal section through stems showing the expression of *NADP-ME2*, *NADP-ME3*, and *NADP-ME4*, respectively. k to m, Staining of inflorescences with flowers of different ages showing the expression driven by *NADP-ME2*, *NADP-ME3*, and *NADP-ME4*, respectively. Anthers expressing GUS in pollen grains are shown in the insets. Scale bars represent 50 μm.

15 (position 2904) and in exon 16 (positions 3141–3144), respectively, were obtained (data not shown). An insertion in intron 16 (positions 3161–3201) in the orientation LB-LB was identified in the line *nadp-me3*. Finally, T-DNAs arranged in tandem repeats with the orientation LB-LB inserted in intron 11 (positions 2041–2054) in *nadp-me4* were confirmed. All lines showed no detectable expression of the corresponding genes as analyzed by RT-PCR using flower cDNA in the cases of *nadp-me2*, *-me3*, and *-me4* and root cDNA in the case of *nadp-me1* (Supplemental Fig. 1). Under greenhouse conditions, normal vegetative and reproductive development for all the single mutants was observed. To test for redundancy, homozygous double mutants were generated between the following pairs: *nadp-me1* and *nadp-me2*, *nadp-me1* and *nadp-me4*, *nadp-me2* and *nadp-me3*, and *nadp-me2* and *nadp-me4*. Also, homozygous triple mutants were generated by crossing the following homozygous lines: *nadp-me1* $\times$ *2* with *nadp-me2* $\times$ *4* and *nadp-me2* $\times$ *3* with *nadp-me2* $\times$ *4*. None of the double- or triple-mutant combinations showed an obvious phenotype under normal growth conditions. A quadruple mutant still could not be isolated.

Contribution of Each Isoform to the NADP-ME Activity in Different Organs of Arabidopsis

To correlate *NADP-ME* mRNA abundance and gene expression patterns with NADP-ME enzymatic activities, Arabidopsis ecotype Columbia (Col-0) and T-DNA insertion mutants were used to analyze the NADP-ME activity using different approaches. Protein extracts from the different lines were assayed for NADP-ME activity and analyzed by native PAGE electrophoresis. In addition, in situ NADP-ME activity staining of 4-week-old plants was performed.

The distribution of NADP-ME activity obtained in different organs of Col-0 and T-DNA insertion mutants is summarized in Figure 7B. In the wild type, as

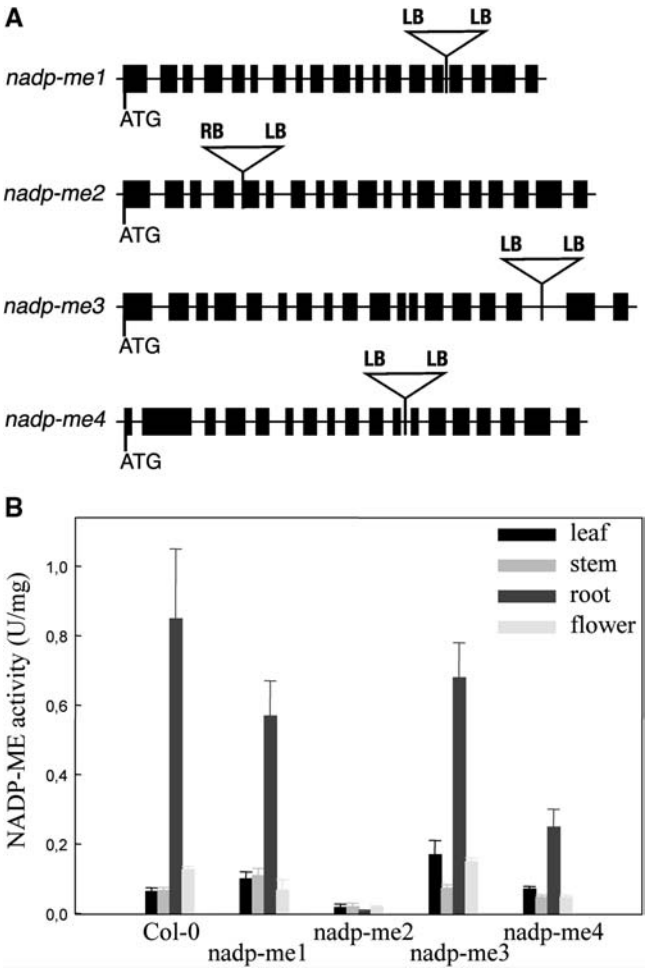

Figure 7. Characterization of nadp-me insertion lines. A, Genomic structure of *AtNADP-ME* genes and location of the T-DNA insertions. Exons are indicated by boxes, whereas introns are represented by lines. The location of the T-DNA insertions in the *nadp-me* lines is indicated by triangles. The orientation of the T-DNA insertions suggests that all the insertions, except that of nadp-me2, present a double inverted repeat. B, NADP-ME activity (units/mg) in different organs of Arabidopsis Col-0 and T-DNA insertion lines. The bars indicate the SD of the measurements from three (in some cases four) different crude extract preparations. The activity measurement was performed three independent times with each crude extract preparation, with less than 5% SD within each preparation.

well as in all the mutants except *nadp-me2*, roots represented the highest specific activities (Fig. 7B). The results obtained indicate that the three *nadp-me2* (*nadp-me2*, *-me2a*, and *-me2b*) knockout mutants display a consistent decrease in NADP-ME activity in all organs tested. In Figure 7B, only the results for line *nadp-me2* are shown, but the other two insertion lines presented the same behavior (data not shown). NADP-ME activity measurements in organs of *nadp-me4* show a significant decrease of activity in flowers and roots. Controversially, the loss of the *NADP-ME3* transcript, which is predominantly expressed in flowers, is accompanied by a significant increase of NADP-ME activity in leaves.

Figure 8A shows results from native PAGE analyses followed by NADP-ME activity staining. In all tissues analyzed, a high molecular mass NADP-ME (>400 kD) can be detected in the wild type. This band may correspond to NADP-ME2 because this isoform is present in all organs (Fig. 2B) and the recombinant purified NADP-ME2 protein possesses this molecular mass as revealed by native PAGE (Fig. 3B). To a lesser extent, NADP-ME1 and -ME3 exhibiting the same molecular mass (Fig. 3B) may contribute to this active band. Two other additional active bands are present in different organs of the wild type, consistent with tetrameric and dimeric states of the enzyme, respectively. These two additional bands are more pronounced in flowers and may correspond to NADP-ME4, because the messenger for this isoform is present in all organs (Fig. 2B) and only the recombinant purified NADP-ME4 protein is present in dimeric and tetrameric states (Fig. 3B). In this way, the oligomeric states observed for the recombinant isoforms are also obtained from Arabidopsis crude extracts.

The high molecular mass active NADP-ME is present in *nadp-me1*, *nadp-me3*, and *nadp-me4*, but is absent in all organs of *nadp-me2* (which is the mutant with the lowest NADP-ME activity in all the organs tested; Fig. 7B), except for flowers (Fig. 8A). This band may represent NADP-ME3, which is predominantly expressed in this organ (Fig. 6l). The lower molecular mass bands, probably due to NADP-ME4 (see above), are visible in all organs of *nadp-me2* and may be responsible for the remaining NADP-ME activity measured. These bands are hardly detected in *nadp-me4*, but visible in both *nadp-me1* and *nadp-me3* (Fig. 8A).

We also performed in situ NADP-ME activity staining of Col-0 and T-DNA insertion mutant seedlings. The results (Fig. 8B) demonstrate that *nadp-me1*, *-me3*, and *-me4* still possess high NADP-ME activity levels, whereas NADP-ME activity is almost absent in *nadp-me2* when compared to the negative control (Col-0 without malate). This result reinforces the idea that the cytosolic NADP-ME2 isoform contributes most to the major global NADP-ME activity, at least in roots and leaves.

DISCUSSION

Arabidopsis Contains Four NADP-ME Isoforms with Different Biochemical and Structural Properties

A comprehensive characterization of the entire NADP-ME family in the C_3 dicot plant Arabidopsis is presented. The presence of both cytosolic and plastidic isoenzymes suggests that the coexistence of both kinds of NADP-MEs may be universal for all plant species, and both kinds of isoforms are also present in the monocot plant rice (Chi et al., 2004). In both plants, an NADP-ME isoform (NADP-ME1) is classified into a new group as detected by phylogenetic analysis (group IV; Fig. 1). None of the group IV members has been characterized so far. The kinetic

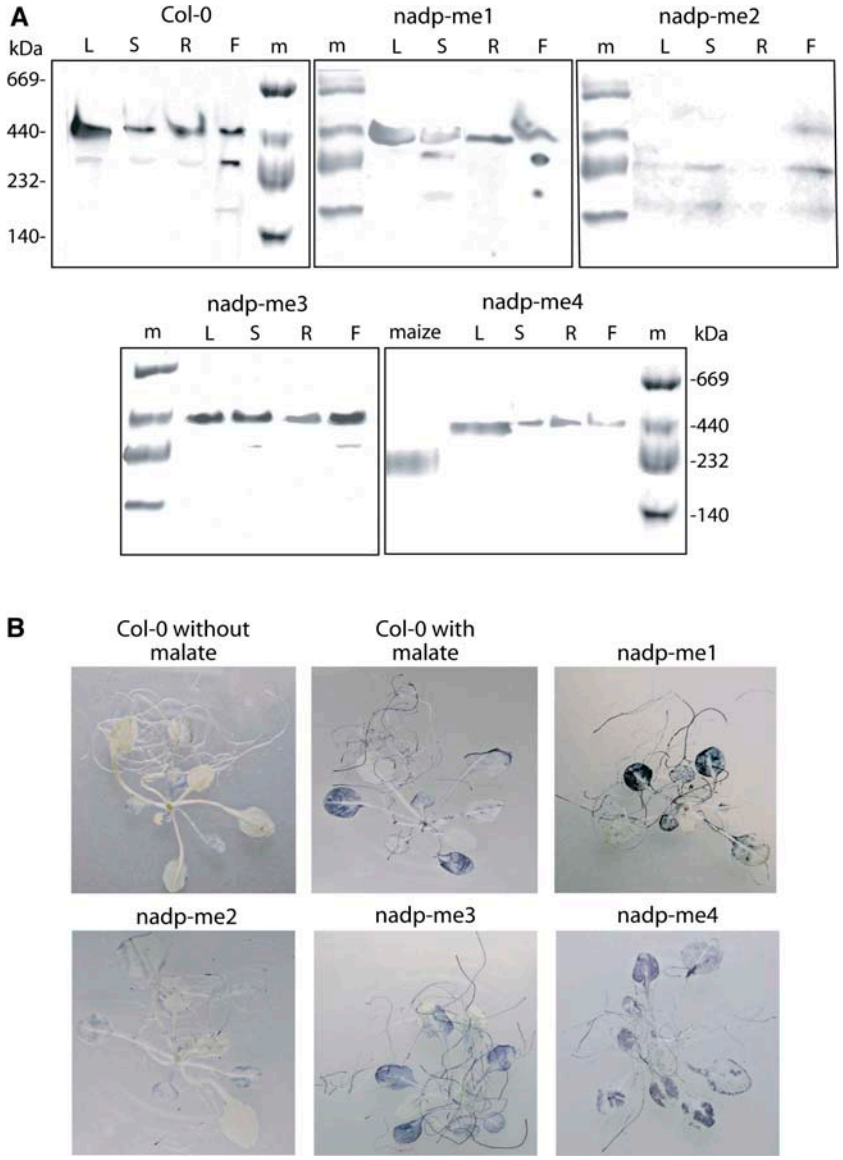

Figure 8. Distribution of NADP-ME activity in different organs of Arabidopsis. A, Native PAGE revealed for NADP-ME activity in different organs of Col-0 and the *nadp-me* lines. Between 2 and 4 milliunits of NADP-ME from different organs (L, leaf, S, stem, F, flower, R, root) were loaded in each case. In the lane indicated as maize, 4 milliunits of NADP-ME from maize leaf crude extract was loaded. m, Molecular mass marker. B, In situ NADP-ME activity assays. Activity staining was performed in 4-week-old Col-0 and *nadp-me* seedlings as described in "Materials and Methods." As a negative control, Col-0 seedlings were incubated in the absence of the substrate L-malate.

and structural properties of the AtNADP-ME1 (Table I; Fig. 3) are very different from the properties of other plant NADP-ME isoforms (Drincovich et al., 2001). The corresponding expression pattern indicates that AtNADP-ME1 is expressed during the late stages of embryogenesis and is restricted to the root tip during germination and to some secondary roots in the mature plant (Figs. 4–6). It is worth mentioning that the maize NADP-ME isoform belonging to group IV exhibits a similar pattern of expression (E. Detarsio, V.G. Maurino, C.S. Andreo, and M.F. Drincovich, unpublished data). Thus, this group may be constituted by NADP-ME isoforms with specific physiological functions during particular developmental stages.

Three putative cytosolic isoforms and one plastidic NADP-ME isoform are expressed in mature tissues of Arabidopsis. Because all three *nadp-me2* are the only insertional mutants with strong decreased levels of NADP-ME activity, it can be suggested that NADP-ME2 is responsible for the major part of NADP-ME activity in mature tissues of Arabidopsis (Figs. 7B and 8B). This isoform, along with the plastidic counterpart (NADP-ME4), are the only isoforms showing a constitutive pattern of expression in Arabidopsis (Figs. 2B and 4–6). On the other hand, the results obtained indicate that the expression patterns of NADP-ME1 and NADP-ME3 are restricted by both developmental and cell-specific signals. These isoforms may play specific roles at particular developmental stages of the plant rather than being involved in the common primary plant metabolism.

Different oligomeric states were observed for the recombinant purified AtNADP-ME isoforms by native gel electrophoresis (Fig. 3B). While the plastidic NADP-ME (NADP-ME4) assembles in equilibrium between dimers and tetramers, the other isoforms are present in a higher oligomeric state (Fig. 3B). In this way, NADP-ME4 resembles the oligomerization pattern

observed for the recombinant maize plastidic photosynthetic (dimer or tetramer, depending on the pH; Detarsio et al., 2003) and nonphotosynthetic NADP-ME (which assembles preferably as a dimer; Saigo et al., 2004). On the other hand, higher molecular mass oligomers have been scarcely observed for NADP-ME isoforms, except the cytosolic CAM NADP-ME from *Mesembryanthemum crystallinum* (Saitou et al., 1992) and the NADP-ME form *E. coli* (Iwakura et al., 1979), both of which were suggested to function as homohexamers. It is worth mentioning that the results obtained about the oligomeric states of the recombinant NADP-MEs are consistent with the patterns observed when analyzing the mutant crude extracts (Fig. 8A); e.g. *nadp-me4* crude extract lacks the lower activity bands. Crystallographic studies of nonplant MEs, i.e. the human mitochondrial NAD(P)-ME (Xu et al., 1999), the pigeon cytosolic NADP-ME (Yang et al., 2002), and the *Ascaris suum* mitochondrial NAD-ME (Coleman et al., 2002), all of which are organized as tetramers, have indicated that some amino acid residues at the carboxyl-terminal region of the enzyme are responsible for their tetrameric state (Chang and Tong, 2003). However, all plant NADP-MEs lack these C-terminal amino acid residues (data not shown) and obviously embark on different strategies for oligomerization.

The kinetic characterization of AtNADP-ME isoforms revealed significant differences (Table I). The k_{cat} obtained for NADP-ME2, NADP-ME3, and NADP-ME4 was very high compared to values previously reported for nonphotosynthetic enzymes (Drincovich et al., 2001). Interestingly, the k_{cat} observed for NADP-ME2 and NADP-ME3 was even higher than the value obtained for maize C_4 NADP-ME (Detarsio et al., 2003). NADP-ME3 exhibits higher affinities for both substrates (malate and NADP) than the other cytosolic isoforms (Table I), and has also the highest catalytic efficiency, which may be in accord with the particular role of this enzyme in specific tissues (Figs. 4–6).

The low K_m (malate) value of the plastidic isoform (NADP-ME4) in relation to values obtained for the cytosolic counterparts, especially NADP-ME1 and NADP-ME2 (Table I), could be explained by the observation that malate concentrations are normally higher in the cytosol than in plastids (Fridlyand et al., 1998). Compared to any other NADP-ME, the kinetic behavior of NADP-ME1 is striking: NADP-ME1 exhibits an extremely high K_m value for NADP and a low k_{cat} in comparison to all recombinant NADP-MEs so far characterized, as well as some kind of sigmoidicity in the kinetics with malate (Table I).

Lack of Obvious Phenotypes of NADP-ME Knockout Mutants at Normal Growth Conditions and Specific Expression Patterns Suggest Different Biological Roles for AtNADP-ME Isoforms

None of the homozygous T-DNA insertional mutants or the double or triple mutants produced showed a phenotype distinguishable from the wild type by growth under normal conditions. The lack of phenotypic defects may be explained by the fact that NADP-ME may be a redundant enzymatic function under normal growth conditions or, alternatively, there may be mutual redundancy of function between isoforms so that no individual isoform is essential. Moreover, we cannot rule out the possibility that there may be a compensatory change in activity of other isoforms when one is removed (Fig. 7B). On the other hand, the distinctive and specific patterns of GUS expression of the members of the AtNADP-ME family during the whole life cycle provide evidence for exclusive roles of each isoform in plant metabolism.

The patterns of expression of NADP-ME4 observed are consistent with the proposed role for NADP-ME in supporting fatty acid synthesis (Smith et al., 1992). In leucoplasts of developing castor seeds, carbon can be incorporated into fatty acids from malate, which supported the highest rate of synthesis in vitro (Smith et al., 1992). It could be suggested that malate could be transported into developing Arabidopsis endosperm leucoplasts, decarboxylated by NADP-ME4, and the resulting pyruvate fed into fatty acid synthesis. After imbibition, GUS expression driven by the *AtNADP-ME* promoters was very high (principally in root tissues), except for *AtNADP-ME3*. Fatty acid biosynthesis is very active in all growing tissues to satisfy the demands for new membrane deposition (Preiss et al., 1994). This makes NADP-ME4 likely to be involved not only in embryogenesis but also in germination. The high level of expression of NADP-ME2 could be correlated with the generation of reducing power in the cytosol for anabolic processes, possibly assisting the oxidative pentose phosphate pathway. In mature organs, the highest NADP-ME activity was found in roots (Fig. 7B), which is consistent with the fact that it is a nonphotosynthetic organ that can use malate as a source of reductant to generate NADPH needed for assimilatory functions.

Recently, C_4 photosynthetic characteristics of cells of stems and petioles that surround the xylem and phloem were reported in tobacco and celery (Hibberd and Quick, 2002). It was shown that malate transported in the xylem can be decarboxylated in chloroplasts of cells bordering the vascular system and the CO_2 released used to produce carbohydrates. The high expression of NADP-ME4 observed in the vasculature of stems and petioles could be linked to this postulated function. In addition to NADP-ME4, NADP-ME2 also showed high expression in cells surrounding the stem vasculature. Both NADP-ME2 in cytosol and NADP-ME4 in chloroplasts could be involved in controlling malate concentration, thus regulating the pH of the xylem. It is also possible that the association of NADP-ME2 with the vasculature reflects its role in providing NADPH for monolignol biosynthesis (Walter et al., 1992). The provision of NADPH for lignin biosynthesis was attributed to the oxidative pentose cycle (Pryke and ap Rees, 1977); however, recruitment of NADP-ME during active growth could be necessary to meet large requirements for NADPH.

In Arabidopsis, trichomes are specialized unicellular structures serving different functions, including the detoxification of cytotoxins and xenobiotics via glutathione conjugation (Gutiérrez-Alcalá et al., 2000). Reducing equivalents for these reactions may be provided by the oxidative pentose phosphate pathway or, alternatively, by the action of NADP-ME. The oxidized form of glutathione is also reduced in these cells by the NADPH-dependent glutathione reductase. Moreover, under toxic zinc and cadmium treatment, increased ME capacity strongly correlated with growth inhibition, as was reported in *Phaseolus vulgaris* (Van Assche et al., 1988). Because NADP-ME3 is highly expressed in trichomes, it might be involved in providing NADPH for these reactions.

Pollen grains accumulate large amounts of intracellular oil bodies that act not only as energy reserves but also as a source for the rapid synthesis of membrane lipids after germination (Piffanelli et al., 1998). In this way, the plastidic NADP-ME4 could be involved in the biosynthesis of fatty acids, a role that is also postulated for this isoform during embryogenesis and germination. It could not be ruled out that mRNAs for NADP-ME3 or NADP-ME4, or both, may accumulate during pollen maturation and translate upon pollen germination (Honys and Twell, 2003). In this case, NADP-ME could be involved in the production of NADPH for the rapid demands during later stages of pollen development.

Concluding Remarks

The characterization of Arabidopsis NADP-ME isoforms indicates different kinetic and biochemical properties and localization patterns for each member of the NADP-ME family. Some isoforms present particular characteristics that may be important to fulfill specific functions, while others are constitutively expressed but are localized to different subcellular compartments. The mutation of any member of the family or their combination did not result in any informative phenotype under greenhouse conditions. It could be possible that NADP-ME may be a redundant enzymatic function under these growth conditions. Alternatively, there may be compensatory changes in activities of other isoforms when one or more are removed. An extensive analysis of the T-DNA insertion mutants under different stress and growth conditions will be of particular interest to reveal the involvement of each NADP-ME isoform in plant metabolism.

MATERIALS AND METHODS

Plant Lines and Growth Conditions

Following cold treatment (72 h at 4°C in the dark), Arabidopsis (*Arabidopsis thaliana*) ecotype Columbia (Col-0) and the T-DNA insertion lines were grown in a greenhouse under a 16-h-light/8-h-dark regime at 22°C. Alternatively, Arabidopsis seedlings were first sown on 0.5× Murashige and Skoog medium (Murashige and Skoog, 1962), containing 1% (w/v) Suc for 2 weeks and then transferred to greenhouse conditions. For in situ enzymatic activity assays, Arabidopsis seedlings were grown on 1× Murashige and Skoog medium containing 3% (w/v) Suc for 4 weeks.

Cloning of AtNADP-ME cDNAs

Total RNA from roots and inflorescences of Arabidopsis was isolated from 100 mg of tissue using the TRIzol reagent (Gibco-BRL). RNA was converted into first-strand cDNA using SuperScript II reverse transcriptase (Invitrogen). Full-length cDNAs were amplified from inflorescence RNA, in the case of *NADP-ME2* and *NADP-ME3*, and from root RNA in the case of *NADP-ME1* and *NADP-ME4*, using platinum Pfx DNA polymerase (Invitrogen) and specific primers. Oligonucleotide primers were designed to introduce unique *Sal*I and *Xho*I sites at the 5′- and 3′-ends, respectively. In order to express the mature NADP-ME4, specific primers containing the first codon downstream of the predicted transit peptide cleavage site (ChloroP V1.1 and TargetP Server v1.01; Emanuelsson et al., 1999) were generated. To amplify *NADP-ME1*, *NADP-ME2*, *NADP-ME3*, and *NADP-ME4* cDNAs, the following primer combinations were used: *Sal*ME1 (5′-ACGTCGACATGGAGAAAGTGACCAACT-3′) and *Xho*ME1 (5′-CTCGAGTCAACGGTAGAGACGGTAT-3′); *Sal*ME2 (5′-GTCGACGAGATATGGGAAGTACTCCGA-3′) and *Xho*ME2 (5′-CTCGAGTTAACGGTAGTTTCTGTACAC-3′); *Sal*ME3 (5′-GTCGACATGGGCACCAATCAGACTCAG-3′) and *Xho*ME3 (5′-CTCGAGTTAACGGAAGTTTCTGTAGCA-3′); and *Sal*ME4 (5′-GTCGACAAATCCACCGTATCTG-3′) and *Xho*ME4 (5′-CTCGAGCTGTTGTATCCTCAGCGGTAG-3′), respectively. The amplified products were cloned into pCR-Blunt II-TOPO (Invitrogen) and sequenced using the PRISM fluorescent dye terminator system (Applied Biosystems).

Generation of Vectors for Expressing the Mature AtNADP-ME Isoforms

The pCR-Blunt II-TOPO plasmids containing the inserts of the different *AtNADP-ME* cDNAs were digested with *Sal*I and *Xho*I and subcloned into the pET32 expression vector (Novagen). The constructs obtained were designed in such a way that, following enterokinase digestion of the chimeric proteins, only a few extra amino acid residues were introduced at the N terminus of the mature proteins.

Heterologous Expression of AtNADP-ME Isoforms

In each pET32 vector containing the inserts of the different *AtNADP-ME* isoforms (pET-ME1, pET-ME2, pET-ME3, and pET-ME4), the NADP-ME is fused in frame to the His-tag in order to facilitate purification of the expressed fusion protein by a nickel-containing His-bind column (Novagen). The induction and purification of the fusion proteins were performed as previously described for the maize (*Zea mays*) photosynthetic and nonphotosynthetic NADP-ME (Detarsio et al., 2003; Saigo et al., 2004). The fusion proteins were then concentrated on Centricon YM-30 (Amicon) using buffer TMG (50 mM Tris-HCl, pH 8.0, 10 mM $MgCl_2$, and 10% [v/v] glycerol). Purified fusion NADP-ME proteins were then incubated with 0.05 to 0.075 units of enterokinase (EK-Max; Invitrogen) per milligram of protein at 16°C for 2 h in order to remove the N terminus coded for by the expression vector. The proteins were further purified using an affinity column (Affi Gel Blue; Bio-Rad). The purified enzyme was stored at −80°C in buffer TMG (with 50% glycerol) for further study.

Protein Crude Extract Preparations

Different tissues (leaf, stem, flowers, and roots) of 6-week-old Arabidopsis wild-type and T-DNA insertion lines were ground in N_2 and the resulting powder was suspended in 100 mM Tris-HCl, pH 7.5, 5 mM $MgCl_2$, 2 mM EDTA, 10% (v/v) glycerol, and 10 mM 2-mercaptoethanol in the presence of a protease inhibitor cocktail (Sigma). The homogenates were clarified by centrifugation and the supernatants were separated for activity measurements or subjected to electrophoresis.

NADP-ME Activity Assays and Protein Concentration Measurement

NADP-ME activity was determined spectrophotometrically using a standard reaction mixture containing 50 mM Tris-HCl, pH 7.5, 10 mM $MgCl_2$, 0.5 mM NADP, and 10 mM L-malate in a final volume of 0.5 mL. The reaction was started by the addition of L-malate. Initial velocity studies were performed by varying the concentration of one of the substrates around its K_m value while keeping the other substrate concentrations at saturating levels. All kinetic parameters were calculated at least by triplicate determinations and

adjusted to nonlinear regression using free concentrations of all substrates (Detarsio et al., 2003). One unit is defined as the amount of enzyme that catalyzes the formation of 1 μmol of NADPH min^{-1} under the specified conditions. Protein concentration was determined by the method of Sedmak and Grossberg (1977) using bovine serum albumin as standard.

Gel Electrophoresis

SDS-PAGE was performed in 10% (w/v) or 7.5% to 15% (w/v) linear gradient polyacrylamide gels according to Laemmli (1970). Proteins were visualized with Coomassie Blue or electroblotted onto a nitrocellulose membrane for immunoblotting. Antibodies against maize recombinant non-C_4 NADP-ME (Saigo et al., 2004) were used for detection (1:100). Bound antibodies were visualized by linking to alkaline phosphatase-conjugated goat anti-rabbit IgG according to the manufacturer's instructions (Sigma). Alkaline phosphatase activity was detected colorimetrically or by using a chemiluminescent kit (Immun-Star; Bio-Rad).

Native PAGE was performed using a 6% (w/v) acrylamide separating gel. Electrophoresis was run at 150 V at 10°C. Gels were assayed for NADP-ME activity by incubating the gel in a solution containing 50 mM Tris-HCl, pH 7.5, 10 mM L-malate, 10 mM $MgCl_2$, 0.5 mM NADP, 35 μg/mL nitroblue tetrazolium, and 0.85 μg/mL phenazine methosulfate at 30°C.

Semiquantitative RT-PCR Analysis

To analyze the expression of the *AtNADP-ME* genes, total RNA from different organs (6-week-old Arabidopsis plants) was isolated and reversed transcribed as stated above. PCR reactions were conducted in a final volume of 10 μL using 0.5 μL of the transcribed product and Taq DNA polymerase (Qiagen). To achieve specific amplification products, one pair of primers was designed for each gene in a way that an intron was spanned in the genomic DNA. The pairs of primers used were as follows: NADP-ME1for (5′-ATGGAGAAAGTGACCAACTCAGA-3′) and NADP-ME1rev (5′-TCGGATATTGTTCAACAGCCTCTTC-3′); NADP-ME2for (5′-ATGGGAAGTACTCCGACTGATTT-3′) and NADP-ME2rev (5′-ACCCGGGTAGTTAACTAATGAGCATCTCT-3′); NADP-ME3for (5′-ATGGGCACCAATCAGACTCAGAT-3′) and NADP-ME3rev (5′-ACCCGGGTATTGTAACGTGGATCACGCAT-3′); and NADP-ME4for (5′-ATGATCTCTCTCACTCCCTCGTT-3′) and NADP-ME4rev (5′-ACCCGGGATCCTGAACTCCACCAGATACGGT-3′). As control, the Actin2 gene was amplified. The primers used were Actin2Sfor (5′-TGTACGCCAGTGGTCCTACAACC-3′) and Actin2Brev (5′-GAAGCAAGAATGGAACCACCG-3′). Amplification conditions were as follows: 3-min denaturation at 94°C; 29 to 35 cycles at 94°C for 30 s, 53°C for 40 s, and 72°C for 30 s, followed by 5 min at 72°C. PCR products were resolved on a 1.5% (w/v) agarose gel.

Generation of *Promoter*::*GUS* Plants

To localize the *NADP-ME* expression in Arabidopsis, promoter regions of all four members of the *AtNADP-ME* family were amplified by PCR and cloned into the *Sma*I-*Hin*dIII or, alternatively, the *Sma*I-*Xba*I sites of the binary vector pGPTV-BAR that carries the *GUS* gene (Jefferson et al., 1987). Oligonucleotide primers were designed to amplify fragments containing a 1.6-kb promoter region upstream of the ATG start codon, the first exon and intron, and a part of the second exon. The primers also introduced respective digestion sites at the 5′- and 3′-ends. The plasmids containing the chimeric *NADP-ME*::*GUS* genes were introduced into Arabidopsis by *Agrobacterium tumefaciens* (GV3101)-mediated transformation using the vacuum infiltration method (Bechtold and Pelletier, 1998). Transgenic lines were selected with BASTA and analyzed for GUS activity (Jefferson et al., 1987). Developmental patterns of promoter activity were analyzed in T2 plants. Siliques at different developmental stages were harvested and excised lengthwise prior to GUS staining. Dissected embryos were cleared in chloralhydrate:water:glycerin (8:2:1) and analyzed under a Nikon eclipse E800 microscope equipped with a digital camera (ky- $F_1$030; JVC).

Construction of the *NADP-ME4*::*GFP* Fusion

The *NADP-ME4*::*GFP* construct contained the first 252 nucleotides of the *NADP-ME4* coding region fused to the *GFP* coding sequence, flanked by the cauliflower mosaic virus 35S promoter and terminator sequences. The selected *NADP-ME4* cDNA region was amplified using the primers NADP-ME4GW for (5′-CACCATGACTCTCTCACTCCCTCG-3′) and NADP-ME4GWrev (5′-ATCCTGAACTCCACCAGATACGGT-3′) and cloned into pENTR/D-TOPO (Invitrogen). GFP fusion constructs were made by subcloning the coding sequence into pGWB5 (for C-terminal GFP), a gateway-compatible binary vector designed for 35S promoter-driven expression of GFP fusion proteins (kindly provided by T. Nakagawa, Shimane University, Izumo, Japan). Cloning using gateway vectors was performed using reagents and protocols from Invitrogen.

Transfection of Tobacco Protoplasts and Microscopic Analysis

Protoplasts were prepared from tobacco (*Nicotiana tabacum*) BY-2 cells and transiently transformed with polyethylene glycol, as described by Negrutiu et al., (1987), using 40 μg of the *35S*::*NADP-ME4*::*GFP* or *35S*::*GFP* and incubated for 24 h in the dark at 25°C before analysis. Epifluorescence microscopy was performed using a Nikon eclipse E800 microscope coupled to a digital camera (ky-$F_1$030; JVC). Detection of GFP was achieved by using a GFP filter (excitation, 460–500 nm; emission, 510–560 nm).

Isolation of T-DNA Insertion Mutants

SALK insertion lines 036898 (*nadp-me1*), 073818 (*nadp-me2*), 020607 (*nadp-me2a*), 139336 (*nadp-me3*), and 064163 (*nadp-me4*) and the insertion line SAIL_752_C09 (*nadp-me2b*) were obtained from the Nottingham Arabidopsis Stock Center (NASC; http://www.arabidopsis.info). The genotype of the lines was determined using a PCR-based approach. Basically, genomic DNA was isolated from individual plants and used as a template for PCR amplifications of wild-type and *nadp-me* alleles. The position of the T-DNA insertion sites into the *nadp-me* genes was verified by amplifying and sequencing the T-DNA flanking genomic DNA.

In Situ NADP-ME Activity Assay

Four-week-old plants were fixed in 2% (w/v) paraformaldehyde and 1 mM dithiothreitol in phosphate-buffered saline, pH 7.0 (0.1% [w/v], Na_2HPO_4, 0.03% [w/v] NaH_2PO_4, and 0.9% [w/v] NaCl) at 4°C for 1 h and then rinsed overnight with water at 4°C (Sergeeva et al., 2004). Staining for NADP-ME activity was performed by submerging the seedlings in a solution containing 50 mM Tris-HCl, pH 7.5, 10 mM L-malate, 10 mM $MgCl_2$, 0.5 mM NADP, 35 μg/mL nitroblue tetrazolium, and 0.85 μg/mL phenazine methosulfate for 90 min at 30°C. The seedlings were destained by soaking in 96% (w/w) ethanol for 1 h at 50°C.

ACKNOWLEDGMENTS

We thank Esther Grube for help in transient GFP expression studies. M.F.D. and C.S.A. are members of the Researcher Career of CONICET, and M.C.G.W. is a fellow of the same institution and Rosario National University.

Received May 19, 2005; revised June 13, 2005; accepted June 13, 2005; published August 19, 2005.

LITERATURE CITED

Arabidopsis Genome Initiative (2000) Analysis of the genome sequence of the flowering plant *Arabidopsis thaliana.* Nature **408:** 795–815

Artus N, Edwards G (1985) NAD-malic enzyme from plants. FEBS Lett **182:** 225–233

Bechtold N, Pelletier G (1998) In planta *Agrobacterium*-mediated transformation of adult *Arabidopsis thaliana* plants by vacuum infiltration. Methods Mol Biol **82:** 259–266

Borsch D, Westhoff P (1990) Primary structure of NADP-dependent malic enzyme in the dicotyledonous *Flaveria trinervia.* FEBS Lett **273:** 111–115

Casati P, Drincovich MF, Edwards G, Andreo C (1999) Malate metabolism by NADP-malic enzyme in plant defense. Photosynth Res **61:** 99–105

Chang G-G, Tong L (2003) Structure and function of malic enzymes, a new class of oxidative decarboxylases. Biochemistry **42:** 12721–12733

Chi W, Yang J, Wu N, Zhang F (2004) Four rice genes encoding NADP malic enzyme exhibit distinct expression profiles. Biosci Biotechnol Biochem **68:** 1865–1874

Coleman DE, Jagannatha Rao GS, Goldsmith EJ, Cook PF, Harris BG (2002) Crystal structure of the malic enzyme from *Ascaris suum* complexed with nicotinamide adenine dinucleotide at 2.3 A resolution. Biochemistry **41:** 6928–6938

Cushman JC (1992) Characterization and expression of a NADP-malic enzyme cDNA induced by salt stress from the facultative Crassulacean acid metabolism plant, *Mesembryanthemum crystallinum.* Eur J Biochem **208:** 259–266

Detarsio E, Gerrard Wheeler MC, Campos Bermúdez VA, Andreo CS, Drincovich MF (2003) Maize C_4 NADP-malic enzyme. Expression in *Escherichia coli* and characterization of site-directed mutants at the putative nucleotide-binding sites. J Biol Chem **278:** 13757–13764

Drincovich M, Casati P, Andreo CS (2001) NADP-malic enzyme from plants: a ubiquitous enzyme involved in different metabolic pathways. FEBS Lett **490:** 1–6

Eastmond PJ, Dennis DT, Rawsthorne S (1997) Evidence that a malate/inorganic phosphate exchange translocator imports carbon across the leucoplast envelope for fatty acid synthesis in developing castor seed endosperm. Plant Physiol **114:** 851–856

Edwards G, Andreo CS (1992) NADP-malic enzyme from plants. Phytochemistry **31:** 1845–1857

Emanuelsson O, Nielsen H, von Heijne G (1999) ChloroP, a neural network-based method for predicting chloroplast transit peptides and cleavage sites. Protein Sci **8:** 978–984

Franke KE, Adams DO (1995) Cloning a full-length cDNA for malic enzyme (EC 1.1.1.40) from grape berries. Plant Physiol **107:** 1009–1010

Fridlyand LE, Backhausen JE, Scheibe R (1998) Flux control of the malate valve in leaf cells. Arch Biochem Biophys **349:** 290–298

Fushimi T, Umeda M, Shimazaki T, Kato A, Toriyama K, Uchimiya H (1994) Nucleotide sequence of rice cDNA similar to a maize NADP-dependent malic enzyme. Plant Mol Biol **24:** 965–967

Gutiérrez-Alcalá G, Gotor C, Myer AJ, Fricker M, Vega JM, Romero LC (2000) Glutathion biosynthesis in Arabidopsis trichome cells. Proc Natl Acad Sci USA **97:** 11108–11113

Hibberd JM, Quick WP (2002) Characteristics of C_4 photosynthesis in stems and petioles of C_3 flowering plants. Nature **415:** 451–453

Honda H, Akagi H, Shimada H (2000) An isozyme of the NADP-malic enzyme of a CAM plant, *Aloe arborescens*, with variation on conservative amino acid residues. Gene **243:** 85–92

Honda H, Shimada H, Akagi H (1997) Isolation of cDNA for an NADP-malic enzyme from *Aloe arborescens.* DNA Res **4:** 397–400

Honys D, Twell D (2003) Comparative analysis of the Arabidopsis pollen transcriptome. Plant Physiol **132:** 640–652

Iwakura M, Hattori J, Arita Y, Tokushige M, Katsuki H (1979) Studies on regulatory functions of malic enzymes. J Biochem (Tokyo) **85:** 1355–1365

Jefferson RA, Kavanagh ZA, Bevan MW (1987) GUS fusions: beta-glucuronidase as a sensitive and versatile gene fusion marker in higher plants. EMBO J **66:** 3901–3907

Laemmli UK (1970) Cleavage of structural proteins during the assembly of the head of bacteriophage T4. Nature **227:** 680–685

Lai LB, Tausta SL, Nelson TM (2002a) Differential regulation of transcripts encoding cytosolic NADP-malic enzymes in C_3 and C_4 *Flaveria* species. Plant Physiol **128:** 140–149

Lai LB, Wang L, Nelson TM (2002b) Distinct but conserved functions for two chloroplastic NADP-malic enzyme isoforms in C_3 and C_4 *Flaveria* species. Plant Physiol **128:** 125–139

Lance C, Rustin P (1984) The central role of malate in plant metabolism. Physiol Veg **22:** 625–641

Laporte MM, Shen B, Tarczynski MC (2002) Engineering for drought avoidance: expression of maize NADP-malic enzyme in tobacco results in altered stomatal function. J Exp Bot **53:** 699–705

Lipka B, Steinmüller K, Rosche E, Borsch D, Westhoff P (1994) The C_3 plant *Flaveria pringlei* contains a plastidic NADP-malic enzyme which is orthologous to the C_4 isoform of the C_4 plant *F. trinervia.* Plant Mol Biol **26:** 1775–1783

Martinoia E, Rentsch D (1994) Malate compartmentation: responses to a complex metabolism. Annu Rev Plant Physiol Plant Mol Biol **45:** 447–467

Maurino VG, Drincovich MF, Casati P, Andreo CS, Ku M, Gupta S, Edwards G, Franceschi V (1997) NADP-malic enzyme: immunolocalization in different tissues of the C4 plant maize and the C3 plant wheat. J Exp Bot **48:** 799–811

Maurino VG, Saigo M, Andreo CS, Drincovich MF (2001) Non-photosynthetic malic enzyme from maize: a constitutively expressed enzyme that responds to plant defence inducers. Plant Mol Biol **45:** 409–420

Murashige T, Skoog F (1962) A revised medium for rapid growth and bioassays with tobacco tissue cultures. Physiol Plant **15:** 473–497

Negrutiu I, Shillito R, Potrykus I, Biasini G, Sala F (1987) Hybrid genes in the analysis of transformation conditions. Plant Mol Biol **8:** 363–373

Outlaw WH, Manchester J, Brown PH (1981) High levels of malic enzyme activities in *Vicia faba* L. epidermal tissue. Plant Physiol **68:** 1047–1051

Piffanelli P, Ross J, Murphy D (1998) Biogenesis and function of the lipidic structures of pollen grains. Sex Plant Reprod **11:** 65–80

Preiss M, Koopmann E, Meyer G, Koyro HW, Schultz G (1994) Malate as additional substrate for fatty acid synthesis in a C_4-plant type developed by salt stress from a C_3-plant type maize. A screening for malate as substrate for fatty acid synthesis in chloroplasts. J Plant Physiol **143:** 544–549

Pryke JA, ap Rees T (1977) The pentose phosphate pathway as a source of NADPH for lignin synthesis. Phytochemistry **16:** 577–560

Rothermel BA, Nelson T (1989) Primary structure of the maize NADP-dependent malic enzyme. J Biol Chem **264:** 19587–19592

Saigo M, Bologna FP, Maurino VG, Detarsio E, Andreo CS, Drincovich MF (2004) Maize recombinant non-C_4 NADP-malic enzyme: a novel dimeric malic enzyme with high specific activity. Plant Mol Biol **55:** 97–107

Saitou K, Agata W, Asakura M, Kubota F (1992) Structural and kinetic properties of NADP-malic enzyme from the inducible Crassulacean acid metabolism plant *Mesembryanthemum crystrallinum* L. Plant Cell Physiol **33:** 595–600

Schaaf J, Walter MH, Hess D (1995) Primary metabolism in plant defense (regulation of a bean malic enzyme gene promoter in transgenic tobacco by developmental and environmental cues). Plant Physiol **108:** 949–960

Sedmak JJ, Grossberg SE (1977) A rapid, sensitive, and versatile assay for protein using Coomassie brilliant blue G250. Anal Biochem **79:** 544–552

Sergeeva LI, Vonk J, Keurentjes JJB, van der Plas LHW, Koornnuf M, Vreugdenhil D (2004) Histochemical analysis reveals organ-specific activities in Arabidopsis. Plant Physiol **134:** 237–245

Smith RG, Gauthier DA, Dennis DT, Turpin DH (1992) Malate and pyruvate-dependent fatty acid synthesis in leucoplasts from developing castor endosperm. Plant Physiol **98:** 1233–1238

Van Assche F, Cardinaels C, Clijsters H (1988) Induction of enzyme capacity in plants as a results of heavy metal toxicity: dose-response relations in Phaseolus vulgaris L., treated with zinc and cadmium. Environ Pollut **52:** 103–115

van Doorsseleare J, Villaroel R, von Montagu M, Inze D (1991) Nucleotide sequence of a cDNA encoding malic enzyme from poplar. Plant Physiol **96:** 1385–1386

Walter MH, Grima-Pettenati J, Grand C, Boudet AM, Lamb CJ (1990) Extensive sequence similarity of a bean CAD4 ''cinnamyl-alcohol dehydrogenase'' to a maize malic enzyme. Plant Mol Biol **15:** 525–526

Xu Y, Bhargava G, Wu H, Loeber G, Tong L (1999) Crystal structure of human mitochondrial NAD(P)-dependent malic enzyme: a new class of oxidative decarboxylases. Structure **7:** 877–889

Yang Z, Zhang H, Hung HH, Kuo CC, Tsai LC, Yuan HS, Chou WY, Chang GG, Tong L (2002) Structural studies of the pigeon liver cytosolic NADP-dependent malic enzyme. Protein Sci **11:** 332–341

Zimmermann P, Hirsch-Hoffmann M, Hennig L, Gruissem W (2004) GENEVESTIGATOR. Arabidopsis microarray database and analysis toolbox. Plant Physiol **136:** 2621–2632